Stabilized detonation for hypersonic propulsion

Daniel A. Rosato[a] , Mason Thornton[a], Jonathan Sosa[b], Christian Bachman[b] , Gabriel B. Goodwin[b], and Kareem A. Ahmed[a,1]

[a]Propulsion and Energy Research Laboratory, Department of Mechanical and Aerospace Engineering, University of Central Florida, Orlando, FL 32816; and [b]Naval Center for Space Technology, US Naval Research Laboratory, Washington, DC 20375

Future terrestrial and interplanetary travel will require high-speed flight and reentry in planetary atmospheres by way of robust, controllable means. This, in large part, hinges on having reliable propulsion systems for hypersonic and supersonic flight. Given the availability of fuels as propellants, we likely will rely on some form of chemical or nuclear propulsion, which means using various forms of exothermic reactions and therefore combustion waves. Such waves may be deflagrations, which are subsonic reaction waves, or detonations, which are ultrahigh-speed supersonic reaction waves. Detonations are an extremely efficient, highly energetic mode of reaction generally associated with intense blast explosions and supernovas. Detonation-based propulsion systems are now of considerable interest because of their potential use for greater propulsion power compared to deflagration-based systems. An understanding of the ignition, propagation, and stability of detonation waves is critical to harnessing their propulsive potential and depends on our ability to study them in a laboratory setting. Here we present a unique experimental configuration, a hypersonic high-enthalpy reaction facility that produces a detonation that is fixed in space, which is crucial for controlling and harnessing the reaction power. A standing oblique detonation wave, stabilized on a ramp, is created in a hypersonic flow of hydrogen and air. Flow diagnostics, such as high-speed shadowgraph and chemiluminescence imaging, show detonation initiation and stabilization and are corroborated through comparison to simulations. This breakthrough in experimental analysis allows for a possible pathway to develop and integrate ultra-high-speed detonation technology enabling hypersonic propulsion and advanced power systems.

oblique detonations | hypersonic propulsion | pressure gain combustion | shock-laden reacting flows | shock-induced combustion

Achieving high-speed flight at supersonic and hypersonic speeds is now a national priority and an international focus. To achieve this ultimate goal, highly energetic propulsion modes are needed to drive the vehicles (1). One set of new concepts, detonation-based engines, could play an important role in making space exploration and intercontinental travel as routine as intercity travel is today (2).

Detonation-based propulsion systems are a transformational technology for maintaining the technological superiority of high-speed propulsion and power systems (3). These systems include gas turbine engines, afterburning jet engines, ramjets, scramjets, and ram accelerators. Detonation is an innovative scheme for hypersonic propulsion that considerably increases thermodynamic cycle efficiencies ($\sim$10 to 20%) as compared to traditional deflagration based cycles (4, 5). Even for applications where there are no additional thermodynamic benefits, detonation-based cycles have shown to provide enhanced combustion efficiency like ram rotating detonation engines (6). Research advancement in ultrahigh-speed detonation systems will help to realize and develop this technological advantage over existing propulsion and power systems.

A detonation is a supersonic combustion wave that consists of a shock wave driven by energy release from closely coupled chemical reactions. These waves travel at many times the speed

of sound, often reaching speeds of Mach 5, as in the case of a hydrogen–air fuel mixture. An engine operating with a Mach 5 flow path corresponds to a vehicle flight Mach number of 6 to 17 (7–9). That is comparable to a half-hour flight from New York to London and is 5 times faster than the average time it took the legendary Concorde to complete the same journey. The idea of using detonation waves for propulsion and energy generation is not new (3), although the implementation of this concept has been difficult. Three main categories of detonation engine concepts have received significant research attention: pulse detonation engines (5, 10–12), rotating detonation engines (13–15), and standing and oblique detonation wave engines (ODWE) (3, 7, 16–18). The ODWE is of particular interest here for its theoretical ability to propel hypersonic aircraft to the speeds needed for spaceplanes and other reusable space launch vehicles. Fig. 1 shows a conceptual hypersonic vehicle powered by an ODWE and illustrates the relation to the experimental and computational results of this study. The challenge in developing these engine concepts is finding reliable mechanisms for detonation initiation and robust stabilization of these waves in the high-speed, high-enthalpy conditions that would be expected of these engine concepts.

Laboratory experiments and numerical simulations have shown a number of modes of detonation initiation, and numerical simulations have elucidated important underlying concepts in their stabilization (19–25). Despite these advances, the problem is compounded by the historical difficulty in achieving a stabilized detonation in an experimental facility that produces realistic flight conditions which can be adapted for use in an actual engine.

Significance

There is now an intensifying international effort to develop robust propulsion systems for hypersonic and supersonic flight. Such a system would allow flight through our atmosphere at very high speeds and allow efficient entry and exit from planetary atmospheres. The possibility of basing such a system on detonations, the most powerful form of combustion, has the potential to provide higher thermodynamic efficiency, enhanced reliability, and reduced emissions. This work reports a significant step in attaining this goal: the discovery of an experimental configuration and flow conditions that generate a stabilized oblique detonation, a phenomenon that has the potential to revolutionize high-speed propulsion of the future.
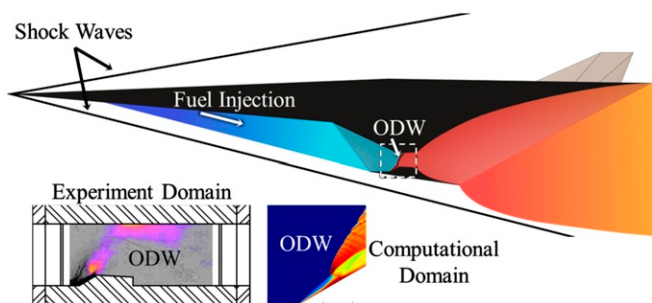
ENGINEERING

Fig. 1. Schematic of oblique detonation engine concept. The experimental and computational ODW domains are highlighted along with their location in the engine flow path.

Previous experimental studies were unable to show a stabilized oblique detonation wave (ODW) for an extended period, due to their use of shock/expansion tubes or projectiles (7, 22, 26–28). These types of facilities have limited run times, on the order of microseconds or milliseconds. Another major difficulty in stabilizing the detonation wave is upstream wave propagation through the boundary layer leading to unstart with recent experiments showing deflagration-to-detonation transition in a hypersonic flow and an unstable detonation that propagated upstream (24). Several numerical studies have shown potentially steady ODW but lack experimental verification (21, 23, 29, 30). These leave uncertainty about the stability of ODW, which must be addressed through experiments capable of creating the appropriate conditions and maintaining them for an extended period.

This paper reports results from a study demonstrating experimentally controlled detonation initiation and stabilization in a hypersonic flow for a situation similar to proposed flight conditions for these vehicle concepts with an active run time of several seconds. The experimental results capture the stabilized detonation, as shown in the shadowgraph and chemiluminescence images, and are further confirmed and explained by the theory and numerical simulations of the system. A 30° angle ramp is used in the high-enthalpy hypersonic reaction facility to ignite and stabilize an ODW, shown schematically in Fig. 2A. The shock-laden, high-Mach number flow induces a temperature rise to ignite and stabilize a detonation in the incoming hydrogen–air mixture. The combination of matching the flow Mach number to the M_{CJ} conditions and low boundary layer fueling result in the stabilized detonation. Static pressure measurements confirm a pressure rise induced by the detonation wave. High-fidelity computational fluid dynamics simulations have been used to provide additional detailed insight into the detonation initiation and stabilization process.

Stabilizing Detonations in a Hypersonic Flow

A detonation is stabilized on a ramp in a hypersonic flow as shown in Fig. 2. The images in the figure show the flow density gradients (shadowgraph) with the chemiluminescence from the chemical reactions overlaid. Fig. 2B shows the baseline nonreacting hypersonic flow in which the preburner was operating and the main fuel injection was not activated leading to no additional chemical reactions in the test section. Fig. 2C shows the same hypersonic flow with the fuel turned on, which resulted in the generation of a stabilized ODW. The hypersonic flow is produced by an axisymmetric Mach 5 converging–diverging nozzle as shown in Fig. 2A. The fuel and air are premixed slightly upstream of the nozzle throat, detailed in *Materials and Methods*. The turning angle of the ramp is $\theta = 30°$. The flow stagnation pressure (P_0) is 5.63 MPa, and the stagnation temperature (T_0) is 1,060 K, resulting in an effective exit Mach number of 4.4, a value expected within the engine flow path of a vehicle fly-

ing at Mach numbers ranging from 6 to 17, largely dependent upon engine inlet design (7–9). The fueled case shown here has a mixture molar composition of major species $H_2/O_2/N_2/H_2O = 13.2/9.3/62.0/14.7\%$ (yielding a global H_2/O_2 equivalence ratio of $\phi_{TS} = 0.71$).

Prior to fueling the facility, the nonreacting flow field was analyzed to confirm the oblique shock wave produced by the ramp matched the theoretical adiabatic oblique shock solution for a 30° ramp. For the given nozzle area ratio ($A/A^* = 25$), the nonreacting hypersonic flow shows the predicted oblique shock angle (β) of 42° for an inflow Mach number of 4.4 with a ratio of specific heats (γ) of 1.3. Once fuel is introduced, an ODW is initiated over the ramp and is sustained for the duration of the experimental test, approximately 3 s. During the reaction, the highest chemiluminescence signal intensity is observed immediately above the ramp due to the presence of the detonation wave at that location. The sustained detonation is shown by the reacting shock structure (RS2) in Fig. 2C. As the incoming flow passes through S2, it enters the induction region. In the induction region, the mixture is heated by the temperature rise across the shock. This heating allows for the reaction process to occur through autoignition and the formation of a detonation wave with a steeper angle, RS2 (73°) (31). The flow velocity is calculated as being 99.7% of the theoretical detonation wave speed for a freely propagating normal detonation in this mixture, U_{CJ}. The static pressure profile shown in Fig. 3D, measured downstream of the ramp, shows a clear pressure rise generated by the reaction when compared to the baseline nonreacting pressure trace over the duration of the test without activating the fuel. The peak pressure reaches 2.7 times the baseline nonreacting pressure and 10.5 times the nozzle exit pressure. The velocity balance and the pressure rise measurements are strong conformation of the detonation formation.

Mechanism of the Oblique Detonation

An ODW is sustained for the duration of active fueling. Fig. 3 shows a sequence of images along with the pressure trace for

Fig. 2. (A) HyperReact. (B) Nonreacting flow field and (C) stabilized ODW.
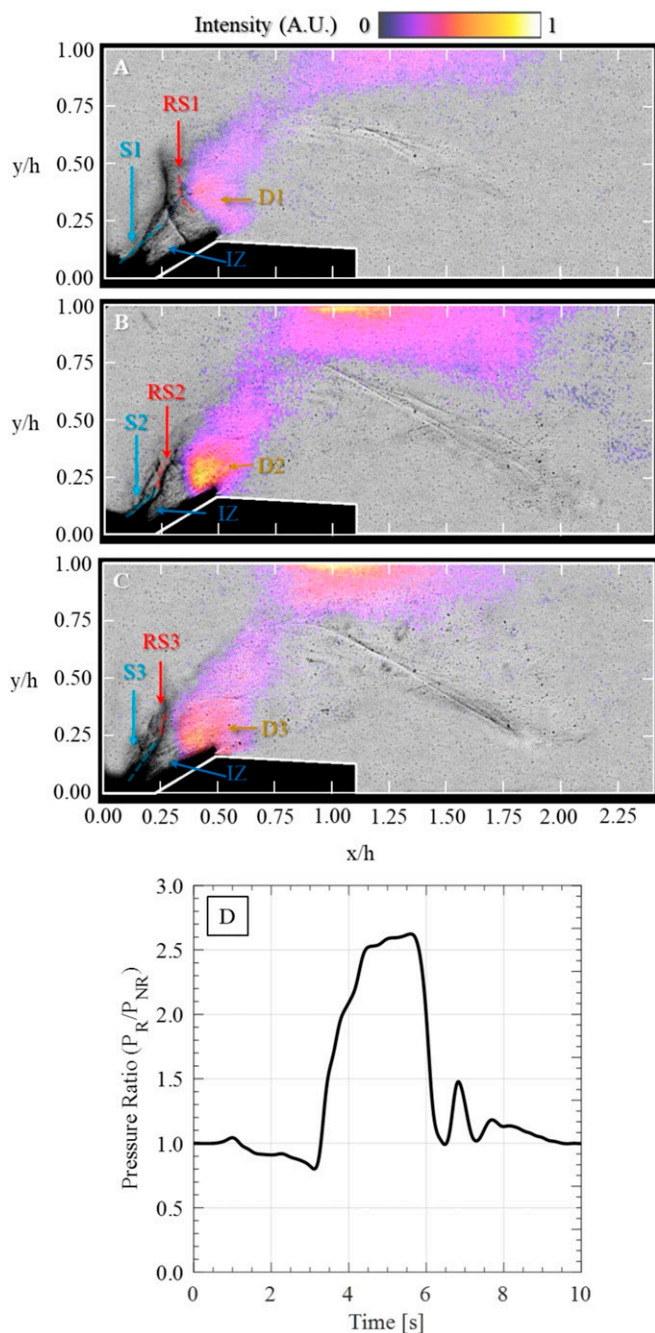
Fig. 3. (*A–C*) The detonation structure for three stages during run and (*D*) reacting test section static pressure ratio (pressure of reacting case [P_R]/pressure of nonreacting case [P_{NR}]) vs. time.

a reacting case. The detonation front remained above the surface of the ramp for the duration of the reaction. While the detonation is sustained, the location of the detonation front fluctuates slightly throughout the run in a cyclical fashion. The shock structure ahead dynamically responds to the fluctuations in the detonation front as seen in the shadowgraph image time series in Fig. 3. The leading reaction front remains at the inflection point between shocks S2 and RS2 while the reactions along the ramp surface cyclically travel upstream and downstream. It is believed that the reaction goes through a cycle-to-cycle variation of underdriven-to-overdriven detonation due to the

turbulent nature of the reacting flow. Additional burning takes place behind the denotative reaction front, above the leading reaction front, and at the top wall. The chemiluminescence signal is filtered to highlight the strongest luminescence emissions that are in visible wavelength range while the broad species occur in the UV wavelength range. Hence, luminescence from the broad species in the test section is not seen in these images.

An important aspect for the detonation wave stability is achieving the ideal balance in mixture composition and heat release for the reaction in the high-Mach number flow. A high heat release will result in a detonation that is overdriven and propagates upstream, opposing to the flow. Conversely, a low heat release will result in the reaction receding downstream and deflagrating. A compressible flow model is used to predict the limits at which ODW stability can be achieved (20). The model generates a theoretical estimate of the range of turning angles and flow Mach numbers over which ODW stability is possible for a given mixture composition, static temperature, and amount of heat release produced by the detonation. The stability band is defined as the conditions that exist on the shock polar, shown in Fig. 4, between θ_{CJ} and θ_{Max}. At a given flow Mach number, θ_{CJ} is the minimum turning angle for which the detonation calculated can be stabilized, and θ_{Max} is the maximum turning angle at which the ODW will remain attached to the ramp. The shock polar originates from the Chapman Jouguet (CJ) Mach number, M_{CJ}, which is the Mach number at which a detonation would freely propagate in a quiescent mixture of the same composition and static temperature. Flow Mach numbers below that value have no stable solution. Because the M_{CJ} value is highly dependent upon the mixture composition, the level of premixing needs to be considered. This was accomplished through H_2 Raman spectroscopy measurement of the fuel profile in the test section, discussed in more detail in *Materials and Methods*. To determine the appropriate M_{CJ} value for this test case, the average local equivalence ratios (ϕ_{TSL_AVG}) from the test section wall to 0.16 times the test section height and from the wall to 0.30 times the test
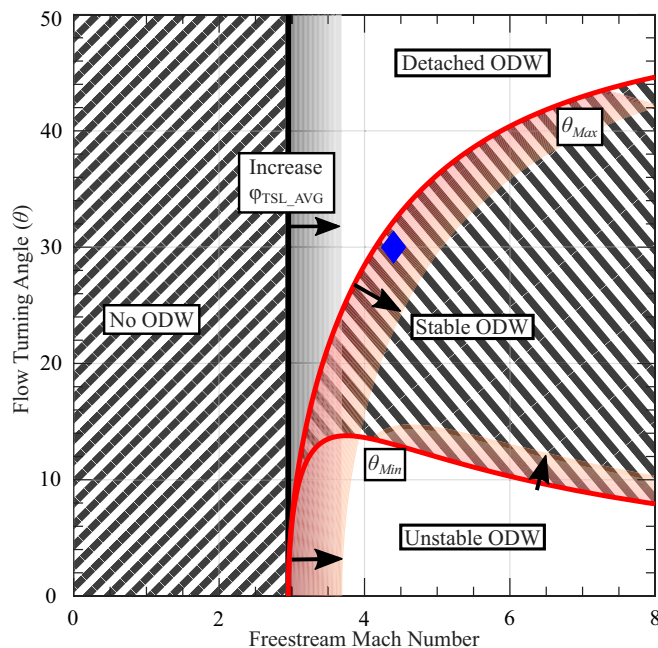

Fig. 4. ODW stability limits. M_{CJ} increases with increasing ϕ_{TSL_AVG}, shifting polar in directions of arrows shown. Solid lines represent conditions for ϕ_{TSL_AVG} = 0.24 with gradients extending to conditions for ϕ_{TSL_AVG} = 0.44. Blue diamond marker represents the test conditions.

ENGINEERING

section height were calculated. These heights correspond to the full height of the ramp and the approximate height at which the reaction and triple point form and were chosen to encompass the fuel most likely to pass through the induction region and detonation wave. For the lower segment, ϕ_{TSL_AVG} was calculated as being 0.24, and for the upper segment, $\phi_{TSL\_AVG} = 0.44$, resulting in local M_{CJ} values of 2.95 and 3.68, respectively. Fig. 4 shows the ODW stability limits with the range for both values highlighted in the red shaded area. The flow Mach number and the ramp angle θ for the experiment do not vary. This places the test condition ($M = 4.4, \theta = 30°$) within the theoretical stability limits created by the shock polars for these conditions.

Numerical Simulations

Numerical simulations were performed at conditions approximating those achieved within the experimental facility in order to corroborate the experimental results and compare, in particular, the structure of the ODW. The simulations solve the reacting Navier–Stokes equations for a compressible fluid by numerical integration with fifth-order accuracy in space and second-order in time on a Cartesian, dynamically adapting computational grid. This method is discussed in detail in ref. 32. The maximum computational cell size is 1.4 mm, and the minimum is 11 μm. The reactions are modeled with a simplified, calibrated chemical-diffusive model (CDM) that uses a single Arrhenius reaction rate to convert reactants to products. The CDM has been used extensively in detonation studies, shown to reproduce desired combustion properties, such as detonation wave speed and flame temperature (33–35), and was used recently to study ODW ignition and stability characteristics when a boundary layer is present on the wedge surface (32). For this study, the CDM was optimized for a hydrogen–air mixture.

The supersonic reactive flow over the ramp was modeled in an idealized way, in a rectangular domain with a diagonal inflow from the left and right boundaries, using a boundary condition on the lower wall to model the flow interaction with the ramp. Thus, the domain and conditions were constructed as if rotated 30° in order to model the ramp angle on an orthogonal mesh, shown in Fig. 5A. The visualization of the results in Fig. 5B has been rotated to the experimental frame of reference and cropped to more accurately represent the experiments.

A snapshot of the numerical result is shown in Fig. 5B, and the same image is overlaid on the experimental shadowgraph in Fig. 5C with the relevant structures aligned. The lack of turbulence present in the simulations compared to its abundance in the experiments necessitated an attempt to make up for local compressibility effects and temperature fluctuations in the experiments by simulating a higher static temperature inflow. This is seen by the minimum temperature bound on the color map in Fig. 5B, which is higher than the static temperature of the fuel–air mixture in the experiments, and was required for ODW initiation in the simulations. In this way, the enthalpy of the incoming fuel–air mixture in the simulations is enhanced beyond that of the experimental facility in order to compensate for the inability of the simulations to reproduce the experiment's turbulence, which has been shown to assist in mixture ignition through the generation of eddy shocklets and local compressibility effects (36). The inflow Mach number is 5 (Mach number generated in the experimental facility after full expansion of an incoming airflow), and the static pressure matches that of the experiments. A burning boundary layer is present due to the great amount of viscous heating that occurs along the no-slip boundary that is imposed on the ramp surface. Above the boundary layer, the freestream passes through an induction region in which the flow autoignites, forming a reaction front which steepens and intersects the leading oblique shock wave. This intersection forms a triple point of extremely high pressure and temperature, out of
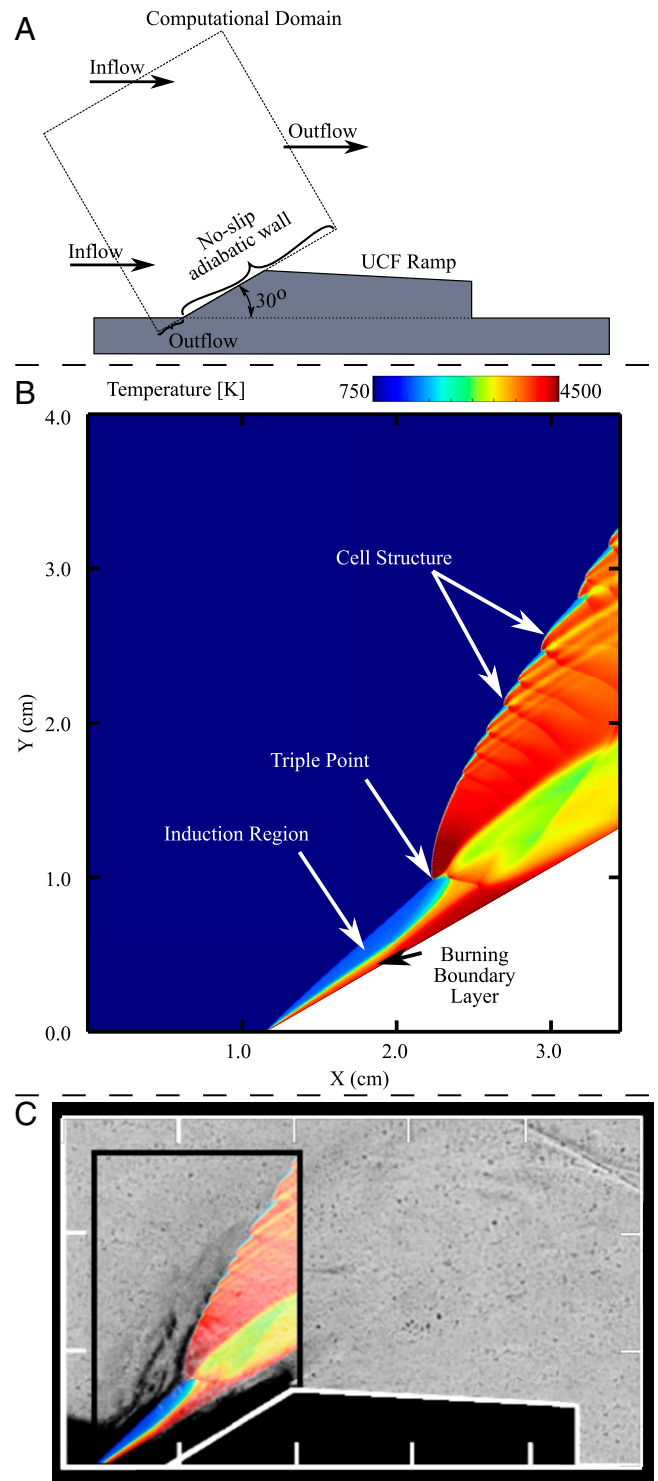

Fig. 5. (A) Computational domain overlaid on test section ramp geometry. (B) Simulation results showing the ODW temperature field. (C) Experimental shadowgraph image of the ODW structure overlaid with simulation results from B.

which propagates an ODW. It is seen in Fig. 5C that the leading oblique shock wave, triple point, and ODW are evident in both experiment and simulation, all of which are important characteristics of the traditional ODW structure. In the simulations, there is clear detonation cell structure, typical of a propagating detonation wave.
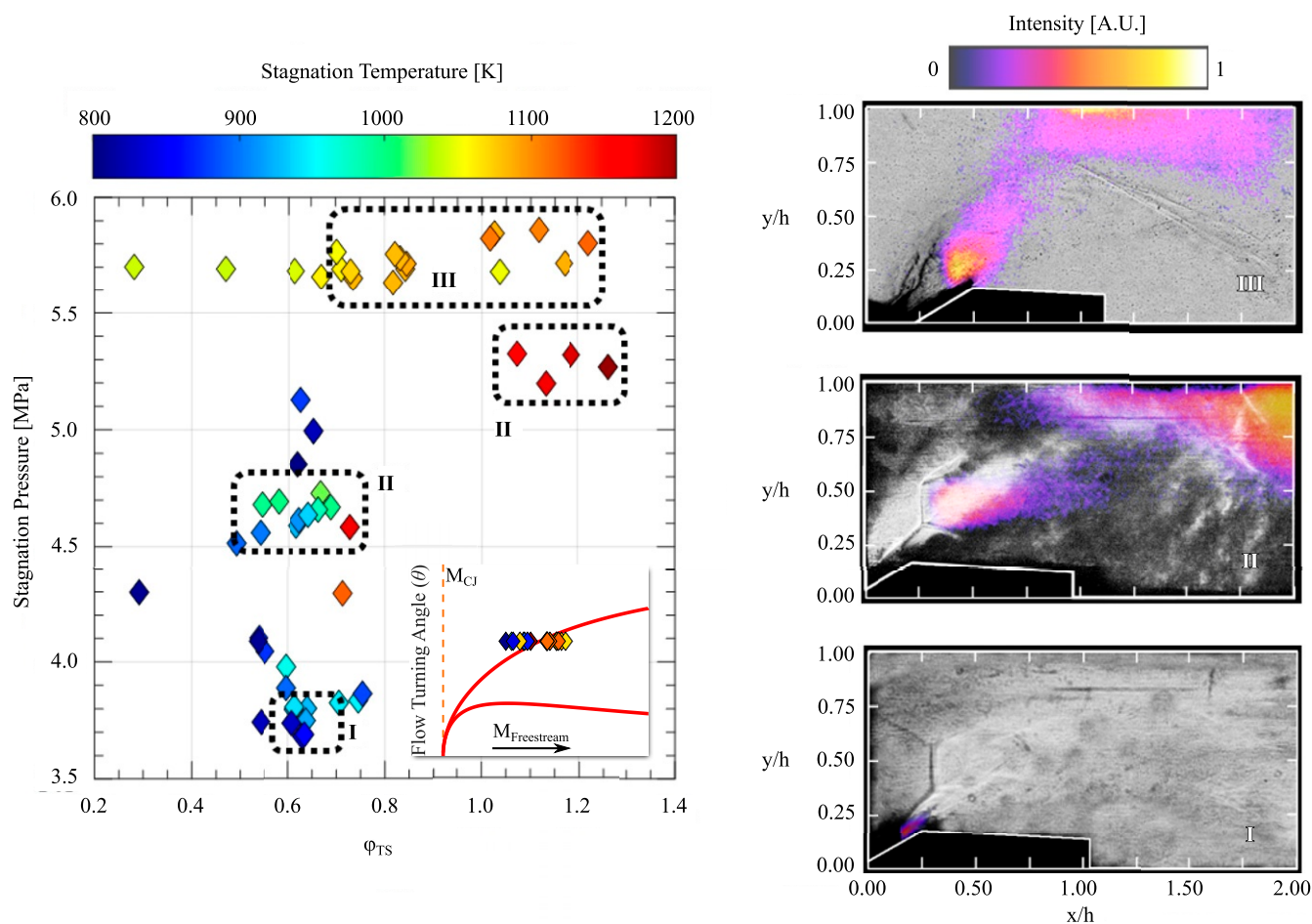
Fig. 6. (*Left*) Operating conditions tested with ramp for $\theta = 30°$ with stability map for the reacting test conditions. (*Right*) Overlaid shadowgraph-chemiluminescence of major modes of operation: regime I, oblique shock-induced combustion; regime II, Mach disk shock-induced combustion; and regime III, ODW.

Hypersonic Reacting Flow Regimes

A large range of conditions were explored in the process of pursuing the stable detonation waves highlighted in this paper. During this process, three major forms of reaction behaviors were observed showing the evolution and the controllability of different burning modes over a broad range of conditions. Fig. 6 shows the conditions tested using the facility. The flow turning angle was held constant at $\theta = 30°$ while the stagnation pressure, stagnation temperature, and mixture composition were varied. At relatively low total temperatures, total pressures, and equivalence ratios, represented by regime I in Fig. 6, deflagrated reactions are experienced over the ramp surface.

As the temperature and pressure are increased, shock-induced combustion occurs. For the cases in regime II, the reaction is oscillatory in nature. Starting from the initiation point on the far wall, the reaction begins to build pressure and propagate forward. The forward-propagating reaction wave intersects with the oblique shock generated by the ramp and forms a Mach disk. A Mach disk is a normal shock with high temperature recovery, enabling higher reaction rates and more rapid heat release leading to an overdriven detonation propagating upstream. The propagation velocity of these reactions exceeds 80% of the CJ detonation velocity. The shock-coupled reaction enters the nozzle and then recedes back downstream to either extinguish or repeat the cycle.

Regime III occurs at the highest tested pressures (5.6 to 5.9 MPa) and total temperatures 1,050 to 1,100 K. A stable oblique

detonation is observed within the test section at ϕ_{TS} values ranging from approximately 0.7 to 1.2. The case used to illustrate the sustained ODW falls within regime III. The additional stagnation pressure in this regime, as compared to all other cases, appears to be the critical factor in establishing a stable ODW at the temperatures and flow Mach numbers of this facility.
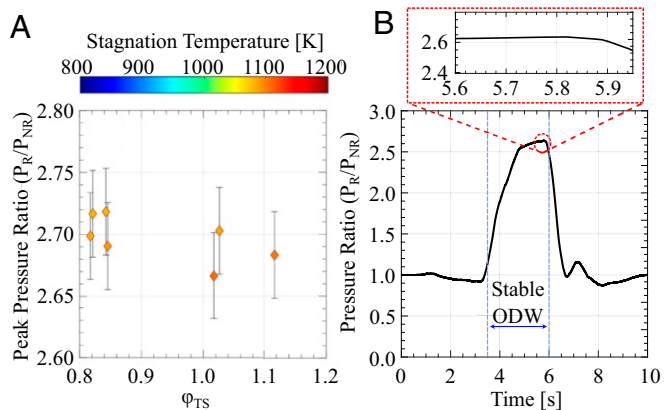

Fig. 7. (*A*) Normalized pressure rise for ODW cases (regime III). (*B*) Regime III average pressure ratio vs. time.

Rosato et al.
Stabilized detonation for hypersonic propulsion

PNAS | 5 of 7
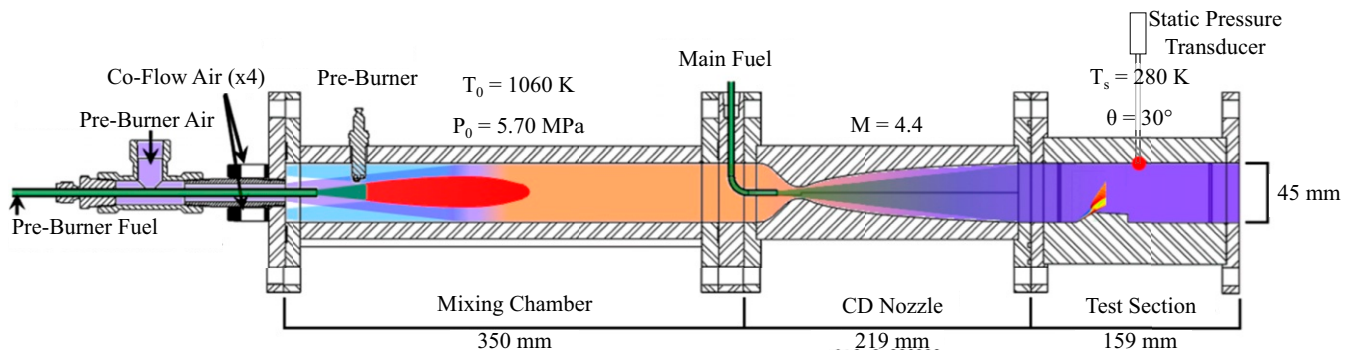https://doi.org/10.1073/pnas.2102244118

Fig. 8. Schematic of HyperReact experimental facility.

Reactions in this regime cause a pressure rise within the test section, as compared to the nonreacting baseline case at similar total pressure and temperature. Fig. 7*A* shows the ratio of the peak test section static pressure during regime III reaction cases with respect to the baseline static pressure. Across regime III, the pressure rise remains at approximately 2.7 times greater than the baseline case. Fig. 7*B* shows the average pressure ratio of all measured regime III cases over the run time. The profile shows a consistent and repeatable pressure rise once the hydrogen fuel is injected.

Materials and Methods

The High-Enthalpy Hypersonic Reacting Facility (HyperReact) at the University of Central Florida (UCF) is used for this study as shown in Fig. 8. The facility consists of five major components which are, in the order of their location along the axial direction of the facility, an in-flow preheater, mixing chamber, main fuel injection stage, converging–diverging (CD) nozzle, and optically accessible test section. The in-flow preheater consists of a coaxial hydrogen–air jet flame surrounded by evenly spaced coflow air jets consuming 44% of the oxygen. The preheater is controlled to achieve a stagnation temperature range of 800 to 1,200 K, corresponding to a static temperature of 180 to 320 K in the test section. The mixing chamber consists of a square channel with an internal height of 45 mm and a length of 350 mm. This segment of the facility allows for homogeneous mixture in-flow feed to the CD nozzle. The main fuel injection used for the downstream reactions introduces the supplementary fuel prior to entering the CD nozzle to allow for premixing. The CD nozzle has an axisymmetric square cross-section along the entire length of the nozzle. The characteristic length scale for the nozzle is the 45-mm height for both the inlet and exit, and the throat height is 9 mm. The inlet-to-throat and exit-to-throat area ratios are both 25:1. The contracting section of the CD nozzle is designed to produce a uniform velocity profile at the throat and minimize boundary layer growth as detailed by Bell and Mehta (37). The diverging section of the nozzle consists of a three-dimensional contour derived from an analytical method by Foelsch (38), and a cubic matching function is used (39) to smoothly transition between the two segments of the nozzle. Additional details on the nozzle design can be found in ref. 40. The CD nozzle is designed to provide an exit Mach number of $M = 5.0$ for dry air at 300 K (24, 40). The effective Mach number is dependent on the temperature and composition-dependent heat capacity ratio of the mixture entering the nozzle for the test, which results in a range of 4.3 to 4.6. The CD nozzle issues the hypersonic flow mixture to the optically accessible test section consisting of a square channel of height 45 mm and length 159 mm. The fuel used for the preheater stage and the main fuel injection is 99.99% ultrahigh-purity hydrogen. Air is provided from a pressure source tank at 34.45 MPa.

Fuel and air mass flow rates supplied to the facility are metered through precision choked orifices. The air orifice is 4.57 mm in diameter. The orifices for the preheater fuel and main fuel injection lines vary in size to accommodate the broad range of fueling flow rates needed to cover the extent of conditions tested. Fuel orifice sizes used range from 0.56 to 1.57 mm in diameter depending on the mixture fraction. Pressures upstream of each choking orifice are measured using Dwyer 626 absolute pressure transducers with ranges of 0 to 20.68 MPa and accuracy of 1% of the full-scale range. The equivalence ratios of both the preburner (ϕ_{burner}) and the downstream conditions in the test section (ϕ_{TS}) are calculated based solely upon the amount

of O_2 and H_2 in the flow at those locations, and the mole fraction of the additional species found is provided in the format (%H_2/%O_2/%N_2/%H_2O). The premixing level of the fuel results in a test section fuel profile that is shown in Fig. 9, which was experimentally determined through Raman spectroscopy measurements during nonreacting operation of the local H_2 concentration. The local premixed mixture equivalence ratio (ϕ_{TSL}) near the ramp surface is then used in calculating ϕ_{TSL_AVG}, defined as being the average fuel concentration between the test section wall at y/h = 0 and the selected upper boundary. ODW characteristics, including M_{CJ} and ODW stability limits, were calculated using the ϕ_{TSL_AVG} values determined by this method.

A 30° turning angle ramp is used for stabilizing the detonation wave. The ramp spanned the full width of test section and is placed at 44 mm downstream of the CD exit plane. The height of the ramp is fixed at 7.5 mm to avoid a blockage ratio higher than 17% within the test section. The aft face of the ramp is relieved at a 3° angle relative to the test section wall. This allows the flow to partially reexpand along its length. Test section static pressure measurements are acquired at the test section's top wall midplane, marked with a red dot in Fig. 8.

The ODW is recorded using simultaneous high-speed schlieren and visible range wavelength 450 to 875 nm chemiluminescence imaging. The test section has fused quartz windows on the side walls for full optical access to an interrogation region of 105 mm long and 45 mm high. The schlieren system consists of a Z-type setup using two 152.4-mm spherical mirrors, with focal lengths of 1.52 m, and a high-power Luminus PT-121-G LED light source. Both the schlieren and chemiluminescence images are captured using Photron SA1.1 high-speed cameras recording at 30 kiloframes
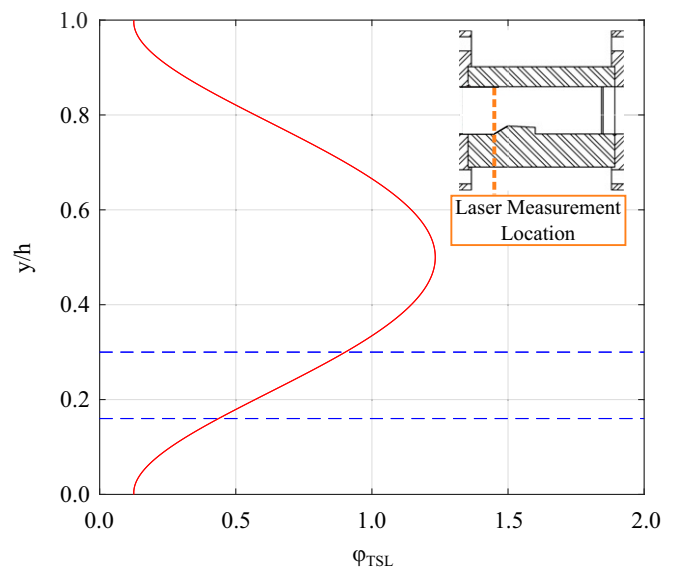

Fig. 9. Schematic of fuel measurement location and curve-fitted local fuel concentration. Limits used to determine ϕ_{TSL_AVG} are also shown.

Rosato et al.
Stabilized detonation for hypersonic propulsion

per second. The schlieren camera is equipped with a Nikon 70 to 300 mm f/4 to f/5.8 lens and images with a 640×288 pixel resolution resulting in a spatial resolution of approximately 164 μm/pixel. The chemiluminescence camera, equipped with a Nikon Nikor 50 mm f/1.2 lens, was operated with a resolution of 350×163 pixels, resulting in an approximate spatial resolution of 300 μm/pixel.

Data Availability All study data are included in the article and *SI Appendix*.

1. H. J. Allen, Hypersonic flight and the re-entry problem: The Twenty-First Wright Brothers Lecture. *J. Aero. Sci.* **25**, 217–227 (1958).
2. R. T. Voland, L. D. Huebner, C. R. McClinton, X-43a hypersonic vehicle technology development. *Acta Astronaut.* **59**, 181–191 (2006).
3. R. Dunlap., A preliminary study of the application of steady-state detonative combustion to a reaction engine. *J. Jet Propuls.* **28**, 451–456 (1958).
4. K. Kailasanath, Review of propulsion applications of detonation waves. *AIAA J.* **38**, 1698–1708 (2000).
5. K. Kailasanath, Recent developments in the research on pulse detonation engines. *AIAA J.* **41**, 145–159 (2003).
6. T. A. Kaemming, M. L. Fotia, J. Hoke, S. A. Schumaker, F. R. Schauer, "Quantification of the loss mechanisms of a ram rotating detonation engine" in *AIAA SciTech 2020 Forum* (AIAA, 2020), p. 0927.
7. P. M. Rubins, R. C. Bauer, Review of shock-induced supersonic combustion research and hypersonic applications. *J. Propul. Power* **10**, 593–601 (1994).
8. G. P. Menees, H. G. Adelman, J.-L. Cambier, "Analytical and experimental investigations of the oblique detonation wave engine concept" (Report No. NASA-TM-102839, NASA Technical Reports Server, 1991) https://ntrs.nasa.gov/citations/19930023185. Accessed 26 April 2021.
9. W. H. Sargent, R. A. Gross, Detonation wave hypersonic ramjet. *ARS J.* **30**, 543–549 (1960).
10. G. D. Roy, S. M. Frolov, A. A. Borisov, D. W. Netzer, Pulse detonation propulsion: Challenges, current status, and future perspective. *Prog. Energy Combust. Sci.* **30**, 545–672 (2004).
11. S. Eidelman, "Pulse detonation engine-a status review and technology development road map" in *33rd Joint Propulsion Conference and Exhibit* (AIAA, 1997), p. 2740.
12. W. H. Heiser, D. T. Pratt, Thermodynamic cycle analysis of pulse detonation engines. *J. Propul. Power* **18**, 68–76 (2002).
13. K. Kailasanath, "The rotating detonation-wave engine concept: A brief status report" in *49th AIAA Aerospace Sciences Meeting Including the New Horizons Forum and Aerospace Exposition* (AIAA, 2011), p. 580.
14. F. K. Lu, E. M. Braun, Rotating detonation wave propulsion: Experimental challenges, modeling, and engine concepts. *J. Propul. Power*, **30**, 1125–1142 (2014).
15. M. Hishida, T. Fujiwara, P. Wolanski, Fundamentals of rotating detonations. *Shock Waves* **19**, 1–10 (2009).
16. E. Dabora, J.-C. Broda, "Standing normal detonations and oblique detonations for propulsion" in *29th Joint Propulsion Conference and Exhibit* (AIAA, 1993), p. 2325.
17. P. Wolański, Detonative propulsion. *Proc. Combust. Inst.* **34**, 125–158 (2013).
18. G. P. Menees, H. G. Adelman, J.-L. Cambier, J. V. Bowles, Wave combustors for trans-atmospheric vehicles. *J. Propul. Power* **8**, 709–713 (1992).
19. R. A. Gross, Oblique detonation waves. *AIAA J.* **1**, 1225–1227 (1963).
20. D. T. Pratt, J. W. Humphrey, D. E. Glenn, Morphology of standing oblique detonation waves. *J. Propul. Power* **7**, 837–845 (1991).
21. Y. Liu, Y.-S. Liu, D. Wu, J-P. Wang, Structure of an oblique detonation wave induced by a wedge. *Shock Waves* **26**, 161–168 (2016).
22. C. I. Morris, M. R. Kamel, R. K. Hanson, "Shock-induced combustion in high-speed wedge flows" in *Symposium (International) on Combustion* (Elsevier, 1998), vol. 27, pp. 2157–2164.
23. F. K. Lu, H. Fan, D. R. Wilson, Detonation waves induced by a confined wedge. *Aerospace Sci. Technol.* **10**, 679–685 (2006).
24. J. Sosa *et al.*, Controlled detonation initiation in hypersonic flow. *Proc. Combust. Inst.* **38**, 7596–7606 (2020).
25. A. Y. Poludnenko, J. Chambers, K. Ahmed, V. N. Gamezo, B. D. Taylor, A unified mechanism for unconfined deflagration-to-detonation transition in terrestrial chemical systems and type IA supernovae. *Science* **366**, eaau7365 (2019).
26. M. J. Kaneshige, J. E. Shepherd, "Oblique detonation stabilized on a hypervelocity projectile" in *Symposium (International) on Combustion* (Elsevier, 1996), vol. 26, pp. 3015–3022.
27. J. Kasahara *et al.*, Criticality for stabilized oblique detonation waves around spherical bodies in acetylene/oxygen/krypton mixtures. *Proc. Combust. Inst.* **29**, 2817–2824 (2002).
28. C. Viguier, L. F. F. Da Silva, D. Desbordes, B. Deshaies, "Onset of oblique detonation waves: Comparison between experimental and numerical results for hydrogen-air mixtures" in *Symposium (International) on Combustion* (Elsevier, 1996), vol. 26, pp. 3023–3031.
29. L. F. F. Da Silva, B. Deshaies, Stabilization of an oblique detonation wave by a wedge: A parametric numerical study. *Combust. Flame* **121**, 152–166 (2000).
30. C. L. Bachman, G. B. Goodwin, K. Ahmed, "Wedge-stabilized oblique detonation waves in a hypersonic hydrogen-air premixed freestream" in *AIAA Propulsion and Energy 2019 Forum* (AIAA, 2019), p. 4044.
31. C. Li, K. Kailasanath, E. S. Oran, Detonation structures behind oblique shocks. *Phys. Fluids* **6**, 1600–1611 (1994).
32. C. L. Bachman, G. B. Goodwin, Ignition criteria and the effect of boundary layers on wedge-stabilized oblique detonation waves. *Combust. Flame* **223**, 271–283 (2021).
33. C. R. Kaplan, A. Özgen, E. S. Oran, Chemical-diffusive models for flame acceleration and transition-to-detonation: Genetic algorithm and optimisation procedure. *Combust. Theor. Model.* **23**, 67–86 (2019).
34. E. S. Oran, V. N. Gamezo, Origins of the deflagration-to-detonation transition in gas-phase combustion. *Combust. Flame* **148**, 4–47 (2007).
35. G. B. Goodwin, E. S. Oran, Premixed flame stability and transition to detonation in a supersonic combustor. *Combust. Flame* **197**, 145–160 (2018).
36. J. Sosa, J. Chambers, K. A. Ahmed, A. Poludnenko, V. N. Gamezo, Compressible turbulent flame speeds of highly turbulent standing flames. *Proc. Combust. Inst.* **37**, 3495–3502 (2019).
37. J. H. Bell, R. D. Mehta, "*Contraction design for small low-speed wind tunnels*" (Report No. NASA-CR-182747, NASA Technical Reports Server, 1988) https://ntrs.nasa.gov/api/citations/19880012661/downloads/19880012661.pdf. Accessed 26 April 2021.
38. K. Foelsch, The analytical design of an axially symmetric laval nozzle for a parallel and uniform jet. *J. Aeronaut. Sci.* **16**, 161–166 (1949).
39. J. C. Crown, W. H. Heybey, *Supersonic nozzle design*, (Report, Naval Ordnance Lab, White Oak, MD, 1950).
40. J. Sosa, K. A. Ahmed, "Design & development of a hypersonic combustor for oblique detonation wave stabilization" in *55th AIAA Aerospace Sciences Meeting* (AIAA, 2017), p. 0371.

ENGINEERING

Rosato et al.
Stabilized detonation for hypersonic propulsion

PNAS | 7 of 7
https://doi.org/10.1073/pnas.2102244118